Nanoscale

PAPER

View Article Online
View Journal | View Issue

Cite this: *Nanoscale*, 2020, **12**, 3701

Simulated revelation of the adsorption behaviours of acetylcholinesterase on charged self-assembled monolayers†

Shengjiang Yang, [a] Jie Liu, [b] He Zheng, [c] Jinyi Zhong [c] and Jian Zhou *[a]

An acetylcholinesterase (AChE)-based electrochemical biosensor, as a promising alternative to detect organophosphates (OPs) and carbamate pesticides, has gained considerable attention in recent years, due to the advantages of simplicity, rapidity, reliability and low cost. The bio-activity of AChE immobilized on the surface and the direct electron transfer (DET) rate between an enzyme and an electrode directly determined the analytical performances of the AChE-based biosensor, and experimental studies have shown that the charged surfaces have a strong impact on the detectability of the AChE-based biosensor. Therefore, it is very important to reveal the behaviour of AChE in bulk solution and on charged surfaces at the molecular level. In this work, the adsorption orientation and conformation of AChE from Torpedo californica (TcAChE) on oppositely charged self-assembled monolayers (SAMs), COOH-SAM and NH_2-SAM with different surface charge densities, were investigated by parallel tempering Monte Carlo (PTMC) and all-atom molecular dynamics simulations (AAMD). Simulation results show that TcAChE could spontaneously and stably adsorb on two oppositely charged surfaces by the synergy of an electric dipole and charged residue patch, and opposite orientations were observed. The active-site gorge of TcAChE is oriented toward the surface with the "end-on" orientation and the active sites are close to the surface when it is adsorbed on the positively charged surface and the tunnel cost for the substrate is lower than that on the negatively charged surface and in bulk solution, while for TcAChE adsorbed on the negatively charged surface, the active site of TcAChE is far away from the surface and the active-site gorge is oriented toward the solution with a "back-on" orientation. It suggests that the positively charged surface could provide a better microenvironment for the efficient bio-catalytic reaction and quick DET between TcAChE and the electrode surface. Moreover, the RMSD, RMSF, dipole moment, gyration radius, eccentricity and superimposed structures show that only a slight conformational change occurred on the relatively flexible structure of TcAChE during simulations, and the native conformation is well preserved after adsorption. This work helps us better comprehend the adsorption mechanism of TcAChE on charged surfaces and might provide some guidelines for the development of new TcAChE-based amperometric biosensors for the detection of organophosphorus pesticides.

Received 28th November 2019,
Accepted 24th January 2020

DOI: 10.1039/c9nr10123c

rsc.li/nanoscale

Introduction

Acetylcholinesterase (AChE, EC 3.1.1.7) is a serine hydrolase and also an α/β hydrolase with high catalytic activity located primarily in the synaptic cleft.[1] Its fundamental function is to catalyze the hydrolysis reaction of the neurotransmitter acetylcholine into choline and acetate[2] for the purpose of terminating the impulse transmission at cholinergic synapses and maintaining the level of acetylcholine in the nervous system. Therefore, the inhibition of AChE bioactivity will lead to the accumulation of acetylcholine in the body, which further causes a series of negative effects on the physiology of the nervous system with serious or fatal consequences.[3] To improve the farm productivity, organophosphorus pesticides

[a]*School of Chemistry and Chemical Engineering, Guangdong Provincial Key Lab for Green Chemical Product Technology, South China University of Technology, Guangzhou 510640, P. R. China. E-mail: jianzhou@scut.edu.cn; Fax: +86 20 87114069; Tel: +86 20 87114069*
[b]*Key Laboratory for Green Chemical Process of Ministry of Education, School of Chemical Engineering and Pharmacy, Wuhan Institute of Technology, Wuhan 430073, P. R. China*
[c]*State Key Laboratory of NBC Protection for Civilian, Research Institute of Chemical Defense, Academy of Military Science, Beijing 102205, P. R. China*
†Electronic supplementary information (ESI) available. See DOI: 10.1039/c9nr10123c

(OPs), including synthetic esters, amides, or thiol derivatives of phosphoric, phosphonic, phosphorothioic and phosphonothioic acids are widely used in agriculture to eliminate or to control agricultural pests.[4,5] However, OPs are also potent inhibitors of the enzyme activity of AChE, which is the vital enzyme for the orderly functioning of the central nervous systems of insects and mammals.[6] So, the residues of OPs in agricultural products (*i.e.*, vegetables and fruits) or drinking water can cause long-term damage to human health even at trace levels,[7] and the OP residue limit should be regulated and controlled strictly. As a result, developing a rapid and reliable quantitative detection method has become increasingly necessary.

Over the past decades, various techniques have been employed to quantitatively analyse OP residues, such as high performance liquid chromatography, gas chromatography,[8] gas chromatography-mass spectrometry,[9] surface enhanced Raman scattering,[10] enzyme-linked immunosorbent assays,[11] and colorimetric assays.[12] These methods presented high performance for the quantitative detection of OPs; however, they also show several shortcomings, such as they are time-consuming, require sample pre-treatment, highly skilled personnel, and expensive instrumentation and could be performed only in laboratories. In contrast, AChE inhibition-based biosensors have been widely applied in environmental monitoring, food safety, pharmaceutical applications and quality control.[13,14] Compared with the traditional analytical methods for pesticide residues, enzyme biosensors have a series of advantages, such as being simple, rapid, ultra-sensitive, low cost, and highly selective and showing low detection limits. The amperometric AChE biosensor detects the concentration change of thiocholine, an electro-active product, which is produced by the hydrolysis of acetylthiocholine. The bioactivity of AChE can be inhibited when OPs are present, and as a result, less thiocholine is produced and the concentration is lower than the reported normal values.[6] Subsequently, the thiocholine concentration change is transformed to a current signal and could be detected by the sensor. Therefore, the AChE-based biosensor can be used to analyze indirectly the OP concentration in food or drinking water with the detection limit ranging from micromolar to pico-molar levels.[15]

For enzyme-based biosensor design and development, the efficient immobilization of an enzyme on the electrode surface is the most crucial step, the bioactivity and structural stability could be improved by controlling the protein orientation and conformation on the solid surfaces.[16] After immobilization, the enzyme's storage stability, response time and reproducibility can be enhanced when compared with those of the free one.[17] In recent years, the immobilization of AChE on different solid materials surfaces (*i.e.*, polymers, silica, gold, carbon nanotubes and graphene)[18–21] with various immobilization methods and strategies, including direct physical adsorption,[22] physical entrapment in sol-gels and polymers,[20,23] covalent attachment and cross-linking,[21,24] have been reported by many researchers. However, the orientations of the immobilized enzymes are usually random and irregular. Moreover, the dominant driving force of protein–particle interactions is not fully understood in early design, and it is not conducive to improving the enzyme activity and biocatalytic efficiency.[25,26] Recently, functionalized nano-materials and single layered two-dimensional (2D) materials, for example, transition metal dichalcogenides (TMDs), including MoS_2 and WS_2,[27] which allow tailoring the solid surface properties (*i.e.*, charge character, surface charged density and hydrophobicity *etc.*) have been applied to study the interaction between a peptide/protein and the particle surface[28,29] with different experiment methods, such as sum frequency generation (SFG) vibrational spectroscopy,[30] attenuated total reflectance (ATR)-FTIR spectroscopy[27] and single-molecule force spectroscopy (SMFS).[31] In particular, the ordered orientation of enzymes was strongly influenced by the charge properties of the surface.[28,32] Previous studies have shown that nano-materials that are decorated with different charged functional groups (*i.e.*, $-NH_2$, $-COOH$, $-SO_3H$ and $-PO_3H_2$) could be a practical tool to control the adsorption orientation and to find the driving forces of protein adsorption.[26,33] Yu *et al.*[28] investigated the efficient immobilization and catalytic activity of AChE on amino functionalized carbon nanotubes (CNT-NH_2); at the same time, the adsorption behaviours of AChE on pristine, carboxyl (–COOH), and hydroxyl (–OH) decorated CNTs were also investigated. They found that a larger amount of AChE adsorbed on the surface of CNT-NH_2 compared with those on the CNT-COOH, CNT-OH and pristine CNT surfaces. The surface of CNT-NH_2 showed a high affinity to acetylthiocholine chloride. The operation process of immobilization was simplified, and the stability and reproducibility were improved. Besides, the best amperometric response was obtained on the AChE/CNT-NH_2/GC electrode and the peak current of AChE/CNT-NH_2/GCE increased more sharply than the increase of the protein amount adsorbed on CNT-NH_2. Then a glassy carbon electrode (GCE) biosensor modified with CNT-NH_2 was successfully employed to detect the pesticides with a low detection limit in real vegetable samples. They concluded that a more favourable orientation of AChE can be obtained on the CNT-NH_2 surface compared to that on other kinds of functionalized CNTs; namely, AChE could be orderly adsorbed on CNT-NH_2 with the active-site gorge orientated and close to the surface of the CNT. This orientation could shorten the distance between the active centre of AChE and the catalytically active site of the electrode surface, and result in faster electron transfer and more efficient reaction. Liu *et al.*[34] researched the immobilization of AChE on the surface of cationic (positively charged) poly(diallyl dimethyl ammonium chloride) (PDDA) functionalized CNTs, and they found that the unique sandwich-like layer-by-lay (LBL) nanostructure (PDDA–AChE–PDDA) formed by self-assembly on the CNT surface provided a favourable microenvironment to maintain the bioactivity of AChE; the PDDA/AChE/PDDA/CNT/GC biosensor improved greatly the electrochemical detection ability for the enzymatically generated thiocholine product, and it was used to monitor OPs and nerve agents (*i.e.*, paraoxon) with excellent performance and showed good precision, reproducibility and stability. Zhang

et al.[35] successfully developed a highly sensitive amperometric AChE-biosensor based on the nanocomposite, which consists of Ag nanoparticles and amino functionalized reduced graphene oxide (Ag–rGO-NH_2), and a conjugated polymer. This biosensor presented excellent conductivity, catalytic activity, biocompatibility, high sensitivity and reproducibility for the analysis of pesticides and acetylthiocholine chloride (ACTI). Similar experimental results have also been reported in a previous study.[36] This indicates that the immobilization of AChE on the surface of an amino functionalized ($-NH_2$) nanomaterial could significantly improve its bioactivity and stability,[28,34–37] and provides a promising approach for the development of enzyme-based biosensors for OPs.

The aforementioned studies on AChE mainly focused on the adsorption amount, catalytic activity and stability after immobilization on different nanomaterial surfaces;[28,34–37] it could be concluded that the characteristics of the interface strongly influenced AChE catalysis. However, detailed information is still limited from experiments, the fundamental microscopic mechanism of AChE adsorption on charged surfaces is not clear and the orientation and conformational changes of AChE on charged surfaces have not been paid sufficient attention yet, which are essential for the bioactivity of enzymes. It is still a technical challenge for the experiment to obtain the orientation and conformation information at the molecular level. In order to completely understand the microscopic enzyme-substrates or enzyme–support interactions, molecular dynamics (MD) simulations, as a powerful complementary tool to experiments, are entirely appropriate for studying the adsorption behaviour of proteins/peptides on solid surfaces at the atomistic level.[38–42] In our previous studies,[43–45] we have demonstrated that the multiscale simulations method, a combination of parallel tempering Monte Carlo (PTMC) algorithm[46] and MD simulations, was a practical approach to study the mechanism of protein adsorption on different solid surfaces. To the best of our knowledge, there are few MD simulation studies on AChE adsorption upon charged solid surfaces.

In this work, the PTMC with a coarse-grained model and all-atom molecular dynamics (AAMD) simulations were used to clarify the binding mechanism of AChE on oppositely charged self-assembled monolayers (SAMs), including carboxyl-functionalized (COOH-SAM) and amino-functionalized (NH_2-SAM) SAMs. Firstly, the PTMC simulations were employed to quickly determine the preliminary preferential orientation of AChE adsorbed on charged surfaces. Then, with these predetermined orientations obtained from PTMC as the start point of simulations, AAMD simulations were further carried out to investigate the adsorption behaviour of AChE on positively charged (NH_2-SAM) and negatively charged (COOH-SAM) surfaces. As the reference system, the behaviour of AChE solvated in bulk solution was also determined. The adsorption orientation and adsorption induced conformation change of AChE on the two charged surfaces will be examined in detail.

Materials and methods

Protein/enzyme

The AChE from Torpedo californica (TcAChE)[47] is employed to study the adsorption mechanism of AChE on charged surfaces, and the initial X-ray diffraction structure of TcAChE (PDB code: 1EA5)[2] with 1.8 Å resolution is obtained from the Protein Data Bank (http://www.rcsb.org/). The enzyme is an ellipsoid-like protein with dimensions ~45 × 60 × 65 Å and belongs to the class of α/β proteins. It consists of a 12-stranded central mixed β-sheet surrounded by 14 α-helices. The active centre is composed of the representative catalytic triad (Ser200-Glu327-His440); the most striking and important structure of TcAChE is the deep and narrow gorge, about 20 Å long, leading to the active site. In this work, the Pymol software[48] combined with CAVER 3.0[49] software package were employed to compute and to visualize the active-site gorge within TcAChE; the structure is shown in Fig. 1A. The corresponding surface electrostatic profile and hydrophobicity maps of TcAChE were calculated

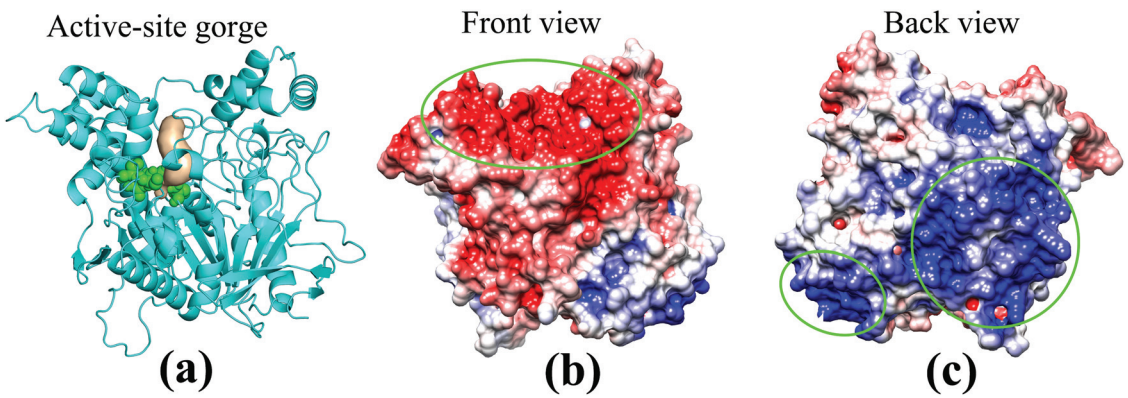

Fig. 1 (A) The secondary structure of TcAChE; the active-site gorge and active sites are represented by the wheat surface and green spheres, respectively. The black arrow (n) and the magenta arrow (d) represent the directions of the surface normal and the electric dipole, respectively. The corresponding front-view (B) and back-view (C) surface electrostatic profiles of TcAChE; the blue, red and white portions signify the positive, negative and neutral potential regions, respectively.

using the UCSF chimera package;[50,51] the electrostatic profile graphs are shown in Fig. 1B (front view) and Fig. 1C (back view) and the hydrophobicity maps are shown in Fig. S3 (including front-view and back-view).† It can be seen that the active-site gorge is mainly composed of a negative potential (the region that is marked by the green circle in Fig. 1B); whereas the opposite side of the active-site gorge consists of a positive potential (Fig. 1C). Furthermore, the electrostatic profile is also demonstrated in Video S1.† The enzyme has 535 residues and its pI is 5.5. The 736 crystal water molecules were reserved from the crystal structure for all simulations, which was critical for maintaining the structure and activity of a protein.[52] Hydrogen atoms within TcAChE were added using the pdb2gmx tool of the GROMACS 4.6.7 software package.[53] The protein was simulated under the physiological conditions and the acidic amino acids (*i.e.*, glutamate and aspartate) and the C-terminus of TcAChE were taken for deprotonation, while the basic amino acids (*i.e.*, lysine and arginine) along with the N-terminus were treated as the protonated state. The protonated state of histidine was calculated using the PDB2PQR and APBS algorithms with the CHARMM force field, at pH 7.0. With this processing, the net charge of TcAChE is found to be $-7e$. The potential parameters for TcAChE were adopted from the CHARMM force field for proteins.[54] In this work, a single protein molecule was employed to investigate the molecular adsorption mechanism (*i.e.*, adsorption orientation, conformation and effective electron transfer) of TcAChE on charged surfaces. It could well reflect the condition of protein solvated in solution at a low concentration or immobilized on the solid material surface with low surface coverage. In the case of high concentration or high surface coverage, interactions between proteins must be considered; the situation is more complicated, which meant that multiple protein molecules (more than one) should be considered in one simulation, and the simulated system will be significantly larger. It leads to the requirement of a computational resource increasing exponentially. However, at present, the computational resource is limited. So, the case of high surface coverage was not considered in this work and it will be considered in our future study with the upgrading of the computational resource.

Surface models

The HS $(CH_2)_{10}NH_2$ SAM and HS $(CH_2)_{10}COOH$ SAM with a $(\sqrt{3} \times \sqrt{3})$ R30° lattice structure[38,55] were employed in all AAMD simulations, representing the positively and negatively charged surfaces, respectively. Each surface includes 396 thiol chains with dimensions of 8.991×9.516 nm^2. In this work, both low surface charge density (SCD, ±0.05 C m^{-2}) and high SCD (±0.19 C m^{-2}) were considered for the COOH- and NH_2-SAMs. Twenty-eight (about 7% dissociation degree) and ninety-nine (about 25% dissociation degree) thiol chains were randomly protonated/deprotonated, representing the SCDs of ±0.05 and ±0.19 C m^{-2}. All sulphur atoms in the SAMs were kept fixed during all simulations; the potential parameters for SAMs were obtained from the CHARMM force field for lipids.[56]

PTMC simulations

In previous studies, researchers have found that a surface-induced conformational change is much slower than the orientation change,[57,58] that is, before the conformational change occurred, the proteins initially experienced a series of translational and rotational motions to adsorb onto the surface with a preferred orientation. Therefore, it is an efficient method to firstly determine the preferred protein orientation on surfaces before MD simulations. In this work, the PTMC algorithm,[46] which is based on the united-residue model,[59] was employed to accurately and efficiently identify the preliminary preferred orientation of TcAChE on different charged surfaces. For the united-residue model for proteins, each amino acid of TcAChE was reduced to a sphere centred at its α-carbon, in which the basic structure information of TcAChE was well kept. During whole PTMC simulations, the protein backbone structure was maintained rigid, and the surface was regarded as a structureless model surface. The potential energy of protein–surface interactions comprises van der Waals (vdW) and electrostatic interaction energies. In our systems, five replicas were set with the temperature distribution of 300 K, 500 K, 800 K, 1500 K and 2500 K to ensure sufficient energy overlap between neighbouring replicas. The swaps are performed every 500 cycles. In each replica, regular MC simulations in a canonical ensemble were carried out in a box of $10 \times 10 \times 10.5$ nm^3. The parameters were adopted from our previous studies.[46,60] Initially, TcAChE was put 5 nm above the model charged surface with a random orientation. During simulations, the protein was translated and rotated around its centre of mass. The displacement of each move was adjusted to ensure an acceptance ratio of 0.5, which is defined as $p(E_i,T_i \rightarrow E_{i+1},T_{i+1}) = \min(1, \exp(\Delta\beta\Delta E))$, where $\Delta\beta = \frac{1}{k_b}\left(\frac{1}{T_{i+1}} - \frac{1}{T_i}\right)$ is the difference between the inverse temperatures of neighbouring replicas, and $\Delta E = E_{i+1} - E_i$ is the energy difference of neighboring replicas; more details could be found from our previous work.[46] In each simulated system, 40 000 000 MC cycles were performed with the former 20 000 000 cycles for equilibrium and the latter 20 000 000 cycles for production analysis. The final preferred configurations of TcAChE obtained from PTMC simulations were taken as the start point for the subsequent AAMD simulations.

AAMD simulations

The GROMACS 4.6.7 software package[53] with the CHARMM force field[61] was employed to carry out all AAMD simulations. The optimized orientations determined from PTMC simulations were adopted as the initial configurations for the following AAMD simulations. At the beginning, TcAChE was placed at 0.6 nm above the SAM surfaces to mimic the pre-adsorbed state. Water molecules, which were described using the TIP3P model,[62] were added to the simulation box with the dimensions of $8.991 \times 9.516 \times 10.5$ nm^3. The added water molecules were selected such that no water oxygen atom was closer than 0.28 nm to the SAM surface and TcAChE. The

counter ions, sodium (Na^+) and chlorine (Cl^-), were added to neutralize the negatively and positively charged SAM systems, respectively. In total, 7 Na^+, 21 Cl^-, 92 Cl^-, 35 Na^+ and 106 Na^+ were added into the bulk, NH_2-SAM (7%), NH_2-SAM (25%), COOH-SAM (7%) and COOH-SAM (25%) systems, respectively. The ionic strength effect was not considered in this work; however, counter ions were added to keep each system neutral, which means that the simulations were performed under the conditions of low ionic strength. Besides, the protein adsorption behaviours at low SCD were contrastively investigated, which could be used to reflect the situation of protein adsorption under high ionic strength conditions to some extent. All AAMD simulations were carried out in an isochoric–isothermal (NVT) ensemble; the time step was 2 fs. The simulated temperature was controlled *via* a Nosé–Hoover thermostat[63] at 300 K with a relaxation constant of 0.5 ps. The particle mesh Ewald (PME) method in a 3dc geometry[64] with a cutoff distance of 1.1 nm was employed to treat the electrostatic interactions. The non-bonded interactions were calculated from a switched potential with a switch function starting at 0.9 nm and reaching zero at 1.0 nm. The LINCS algorithm[65] was used to constrain all bonds including hydrogen atoms. Pseudo-two-dimensional (x and y directions) periodic boundary conditions were used for all protein–surface systems. In the z direction, two hard walls were placed at the top and the bottom of the simulation box; the scaling factor for the z direction for Ewald summation was 3.[53] As a reference system, TcAChE in the aqueous solution was also studied, and three-dimensional (x, y, and z directions) periodic boundary conditions were adopted. For all simulations, the neighbour list was updated every 10 steps. For each system, 200 ns AAMD simulation was performed. Snapshots of all systems were recorded every 10 ps for the following result analysis by using various post-processing tools of GROMACS.[53] All simulation results were visualized using the Pymol software[48] and the visual molecular dynamics (VMD) program.[66]

Table 1 Interaction energies between TcAChE and charged surfaces by AAMD

System	U_{tot} [a] (kJ mol^{-1})	U_{ele} (kJ mol^{-1})	U_{vdW} (kJ mol^{-1})
NH_2-SAM (7%)	−1010.3 ± 98.6	−879.3 ± 85.2	−131.0 ± 31.3
NH_2-SAM (25%)	−1204.3 ± 90.5	−1044.9 ± 87.1	−159.4 ± 29.7
COOH-SAM (7%)	−902.3 ± 97.4	−773.5 ± 74.6	−128.8 ± 39.4
COOH-SAM (25%)	−818.9 ± 89.3	−702.5 ± 83.5	−116.4 ± 26.7

[a] U_{tot} represents the sum of electrostatic and vdW interactions.

Table 2 The averaged properties of the main substrate tunnels within TcAChE adsorbed on charged SAM surfaces by AAMD simulations

System	Tunnel length (nm)	Radius of the tunnel bottleneck (nm)	Tunnel curvature	Tunnel cost
Bulk	1.211	0.191	1.167	0.300
NH_2-SAM (7%)	1.374	0.221	1.147	0.202
NH_2-SAM (25%)	1.372	0.223	1.151	0.202
COOH-SAM (7%)	2.197	0.114	1.761	0.691
COOH-SAM (25%)	1.703	0.155	1.640	0.511

Results and discussion

In this work, the adsorption behaviours of TcAChE on oppositely charged SAMs (COOH-SAM and NH_2-SAM) at different SCDs (±0.05 and ±0.19 C m^{-2}) were studied by performing PTMC and AAMD simulations at the molecular level. For comparison, behaviours of TcAChE in the bulk solution were also investigated. The optimal orientation, interaction energies between TcAChE and SAM surfaces, the binding sites, gyration radius, eccentricity, the root-mean-square deviation (RMSD), superimposed structures and dipole moment of TcAChE from AAMD simulations are discussed in detail. The simulation results were obtained by averaging over the last 60 ns AAMD trajectories, and are summarized in Tables 1–3 and Fig. 2–8.

Adsorption orientation and interaction energy

The adsorption orientation of enzymes on solid materials surfaces was vital for exerting their bioactivities, which determined the distance of electron transfer between the active centre of a protein and the electrode in enzyme-based biosensors and biofuel cells. As reported in previous studies,[67,68] the efficient direct electron transfer (DET) between the redox active site of an enzyme and the electrode surface is a crucial process in biofuel cells and biosensors, because the electrons can transfer directly from the electrodes to the substrate *via* the redox active centre of the enzyme without any redox mediators in the process of DET. In this work, the orientations of TcAChE on oppositely charged surfaces are quantitatively characterized using the orientation angle (θ),[38,44,45,60] which is defined as the angle between the unit vector along the electric dipole of the protein and the unit vector normal to the surface (as shown in Fig. 1A), and the cosine value of this angle is

Table 3 Averaged properties of TcAChE adsorbed on charged surfaces and in bulk solution

	Orientation ($\cos\theta$)	R_{gyr} (nm)	Eccentricity	RMSD (nm) (back-bone)	RMSD (nm) (all-atom)	Dipole (D)
Bulk	—	2.33 ± 0.006	0.18 ± 0.003	0.20 ± 0.015	0.25 ± 0.014	1976 ± 46
NH_2-SAM (7%)	0.81	2.35 ± 0.005	0.18 ± 0.002	0.22 ± 0.009	0.27 ± 0.008	2130 ± 52
NH_2-SAM (25%)	0.92	2.33 ± 0.005	0.17 ± 0.002	0.18 ± 0.008	0.24 ± 0.006	2279 ± 52
COOH-SAM (7%)	−0.90	2.32 ± 0.006	0.17 ± 0.003	0.16 ± 0.009	0.21 ± 0.008	2051 ± 48
COOH-SAM (25%)	−0.92	2.33 ± 0.005	0.18 ± 0.002	0.20 ± 0.010	0.26 ± 0.008	2113 ± 50

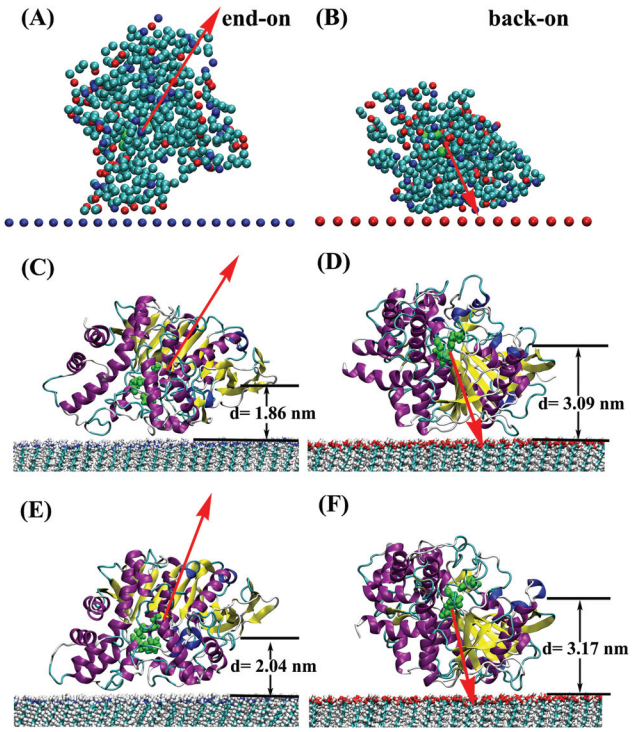

Fig. 2 Adsorption configurations of TcAChE on different charged SAMs from PTMC (A and B) and AAMD simulations (C, D, E, and F): (A) on the positively charged surface; (B) on the negatively charged surface; (C) on the 7% dissociated NH_2-SAM; (D) on the 7% dissociated COOH-SAM; (E) on the 25% dissociated NH_2-SAM; and (F) on the 25% dissociated COOH-SAM. The red arrow indicates the direction of the dipole. Active sites are represented in green beads. The value of *d* indicates the distance between the centre of mass of active sites and SAM surfaces.

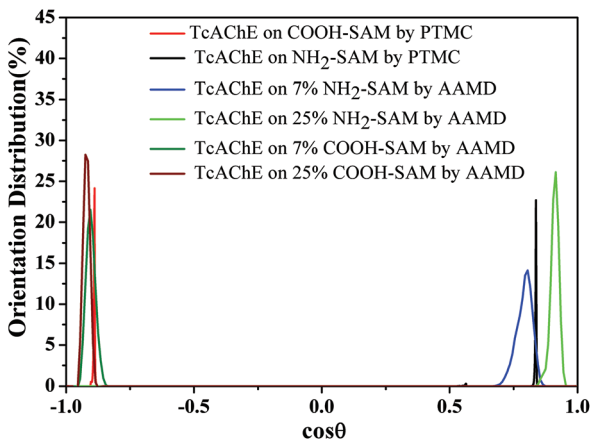

Fig. 3 Orientation distribution of TcAChE adsorbed on oppositely charged surfaces by PTMC and AAMD simulations.

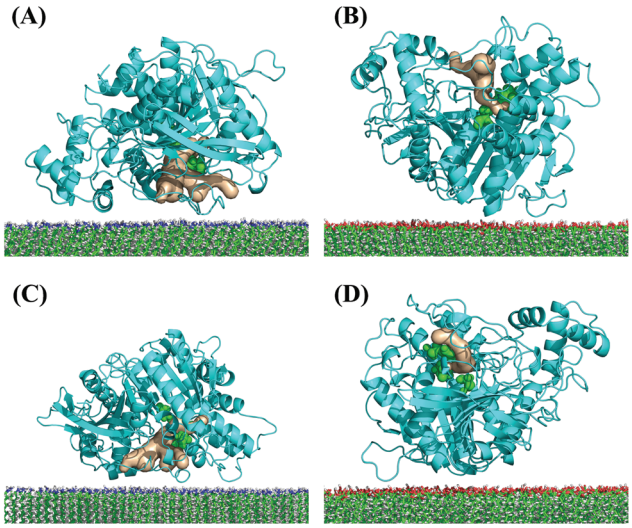

Fig. 4 The final active-site gorge configurations of TcAChE adsorbed on both charged SAM surfaces in AAMD simulations: (A) on the 7% dissociated NH_2-SAM; (B) on the 7% dissociated COOH-SAM; (C) on the 25% dissociated NH_2-SAM; and (D) on the 25% dissociated COOH-SAM. The green spheres and wheat surfaces indicate the active site and active-site gorge, respectively.

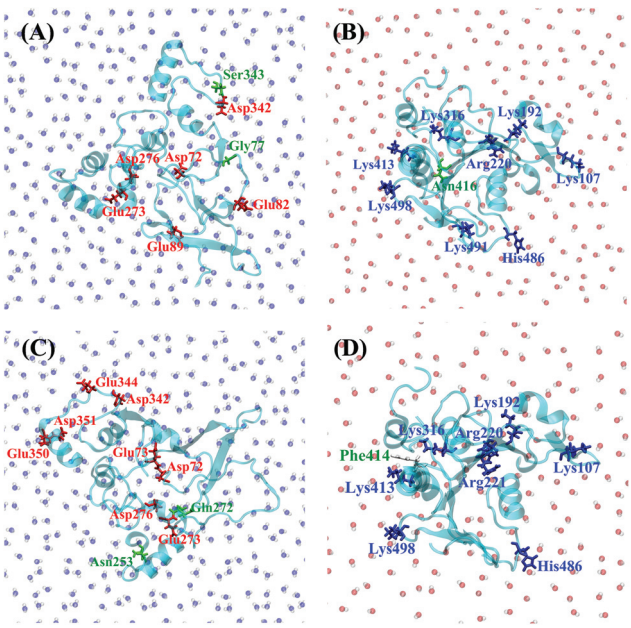

Fig. 5 Top-view snapshots of the key binding sites of TcAChE adsorbed on positively and negatively charged surfaces from AAMD: (A) on the 7% dissociated NH_2-SAM; (B) on the 7% dissociated COOH-SAM; (C) on the 25% dissociated NH_2-SAM; and (D) on the 25% dissociated COOH-SAM. The key residues are shown in the Licorice model. Positive, negative and neutral residues are shown in blue, red and green colours, respectively.

employed to represent quantitatively the orientation of TcAChE on charged SAM surfaces.

Firstly, PTMC simulations were carried out to obtain the preliminary orientations of TcAChE adsorbed on the oppositely charged surfaces. Then, with these orientations used as the starting configurations, AAMD simulations were further performed to investigate the atomistic adsorption behaviours of TcAChE on both charged SAMs (COOH-SAM and NH_2-SAM). The effects of different charged surfaces on the TcAChE

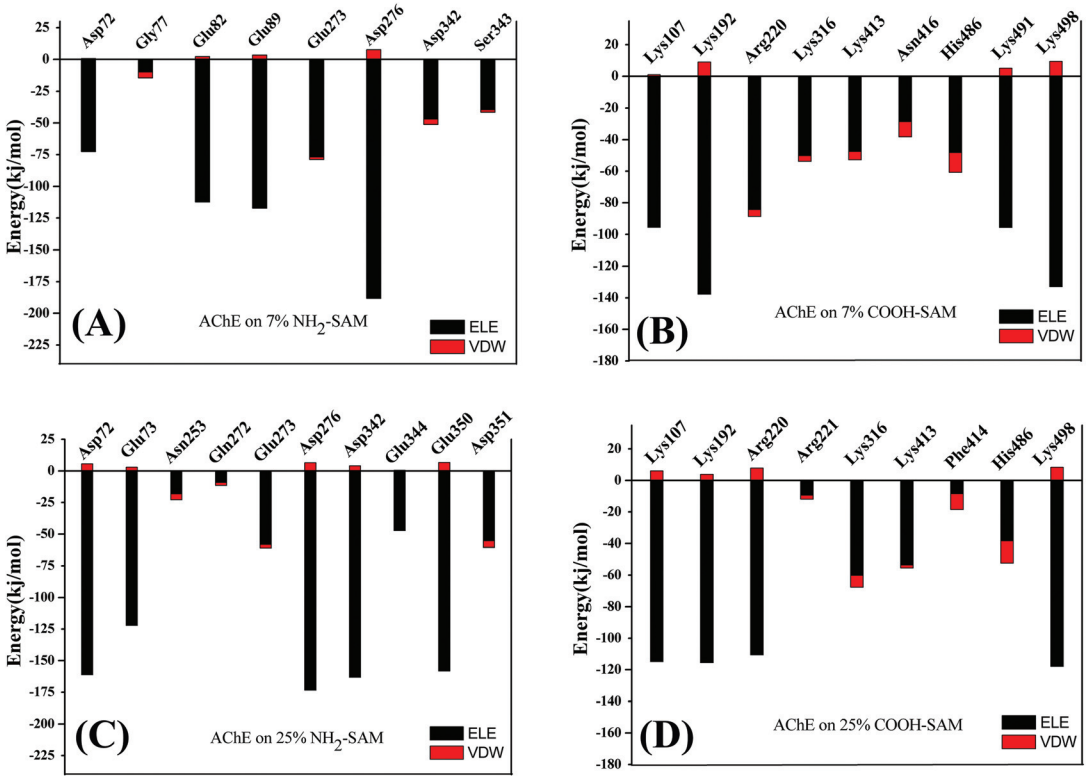

Fig. 6 Electrostatic and vdW interaction energies between the key contact residues of TcAChE and charged surfaces: (A) the 7% dissociated NH_2-SAM; (B) the 7% dissociated COOH-SAM; (C) the 25% dissociated NH_2-SAM; and (D) the 25% dissociated COOH-SAM.

adsorption orientation were analysed in detail. The dominant orientation and the corresponding orientation distribution from PTMC and AADMD simulations are shown in Fig. 2 and 3.

As shown in Fig. 2 and 3, on the 7% and 25% dissociated NH_2-SAM surfaces, the peak values of $\cos\theta$ for TcAChE are 0.81 and 0.92 with the almost symmetrical orientation distributions ranging from 0.70 to 0.87 and 0.85 to 0.95, respectively. This indicates that the trends of orientation distribution of TcAChE adsorbed on NH_2-SAM surfaces with various dissociation degrees are basically the same and the numbers of contact residues (<0.35 nm) are also equal (as shown in Table S1†). However, the orientations of TcAChE adsorbed on charged surfaces with different SCDs are not exactly the same, which leads to the key binding residues which have relatively strong interactions with the charged surfaces being slightly different (as shown in Fig. 6a and c). Moreover, TcAChE has a narrower distribution of the dipole orientation angle and a larger value of $\cos\theta$ (0.91) on the NH_2-SAM surface with a higher SCD; and the dipole direction of TcAChE is almost vertical to the surface. This indicates that a positively charged surface with the relatively high SCD can maintain a more oriented configuration of TcAChE. On the 7% and 25% dissociated COOH-SAM surfaces, TcAChE presents almost the opposite orientation compared with that on the NH_2-SAM surface, and the peak values of $\cos\theta$ are −0.90 and −0.92, respectively. The distributions of dipole angles are almost the same, ranging from about −0.95 to −0.84. This indicates that the changes of the SCD of negatively charged SAMs have no distinct effect on the adsorption orientation of TcAChE. Furthermore, the main negative potential patch (Fig. 1B) and positive potential patch (Fig. 1C) are adsorbed directly on positively charged (NH_2-SAM) and negatively charged (COOH-SAM) surfaces, respectively. Under the regulation of the electric dipole and the distribution of charged patches, TcAChE steadily adsorbs on both charged surfaces, and a similar case can be found in our previous studies;[45,60] this is also consistent with the previous computed results, where the researcher concluded that the protein adsorption behaviour on charged surfaces was based on two mechanisms, *i.e.*, charge regulation and charge-patches,[69] and the orientation of the enzyme on the charged surface is also related to the ionic strength and SCD.[70] Furthermore, the orientation of an adsorbed protein was controlled by both electric and hydrophobic dipoles; that is, the electric dipole played a dominant role on charged surfaces while on hydrophobic surfaces, the hydrophobic dipole played the dominant role.[71,72] Moreover, the hydrophobic surface often caused serious secondary structural changes on the protein/peptide, which further led to a sharp decrease or even denaturation of the bioactivity of the enzyme.[73,74] As shown in Fig. 3, the orientation distribution and adsorption orientation of TcAChE on NH_2-SAM and COOH-SAM surfaces from AAMD simulations all show slight shifts compared with those from PTMC simulations. A highly concentrative orien-

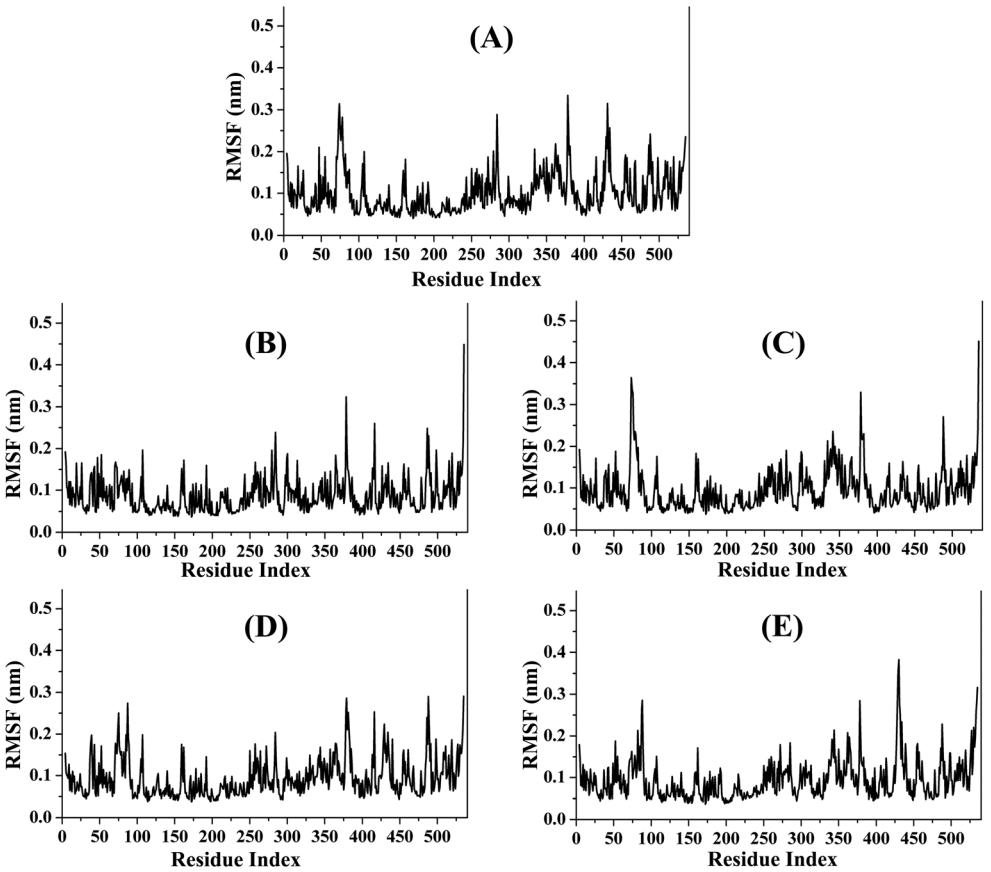

Fig. 7 RMSF of each residue of TcAChE in bulk water (A) and that adsorbed on charged surfaces: (B) on the 7% dissociated NH_2-SAM; (C) on the 7% dissociated COOH-SAM; (D) on the 25% dissociated NH_2-SAM; and (E) on the 25% dissociated COOH-SAM. Residues 1 and 535 represent the N-terminal and C-terminal, respectively.

tation distribution can be obtained in the PTMC algorithm, which is caused by the fact that PTMC simulations were based on the united-residue model, in which the side chains of protein residues are ignored and only the locations of α-C are considered; however, in AAMD simulations, all atoms were taken into account, and in spite of that, the final dominant configurations (Fig. 2) and orientation distributions (Fig. 3) in both PTMC and AAMD simulations presented the same trend.

It can be seen from Fig. 2 that TcAChE could adsorb on NH_2-SAM surfaces with the "end-on" orientation, with the active site orienting toward the surface. This is more beneficial for the DET between TcAChE and electrode surfaces with the active centre close to the electrode surface modified with positive charges. However, on COOH-SAM surfaces, TcAChE is adsorbed with the "back-on" orientation, and the active site is far from the electrode surface, which is unfavourable for the DET process of the TcAChE-based biosensor. This indicates that the immobilization of TcAChE on the positively charged surface is a practicable and effective method to enhance its catalytic activity and the rate of DET, which is consistent with previous experimental results.[28,34,35] As Yu *et al.*[28] found that the catalytic activity, reproducibility and stability of TcAChE were obviously improved after immobilizing on the amine-functionalized ($-NH_2$) carbon nanotube surfaces and the best amperometric response could be obtained when compared with those of TcAChE immobilized on carbon nanotubes modified with carboxyl (–COOH) and hydroxyl (–OH) groups. Liu *et al.*[34] also found that the cationic poly(diallyl dimethyl ammonium chloride) (PDDA, positively charged) functionalized carbon nanotube could enhance the biological activity of TcAChE. Furthermore, Zhang *et al.*[35] reported that the immobilization of TcAChE on an amine functionalized ($-NH_2$) nanomaterial could significantly improve its bioactivity and stability.

Furthermore, to clarify the adsorption strength and modes of TcAChE on charged surfaces, the total protein–surface interaction energies (the interaction energies between the protein and the surface) over the last 60 ns of the AAMD simulation were calculated, and the results were listed in Table 1.

It can be observed that the adsorption behaviour of TcAChE on both charged SAM surfaces is mainly driven by the synergy of electrostatic and vdW interactions, while the electrostatic interaction energies are distinctly higher than vdW interaction energies (as shown in Table 1), which indicates that the electrostatic interactions usually play the dominant role in the process of protein adsorption on charged surfaces, and the same phenomenon was also found in our previous

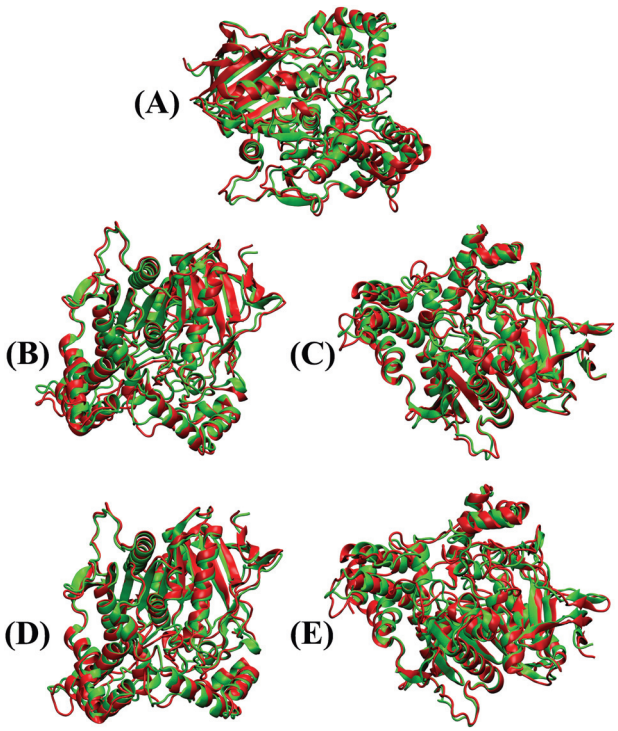

Fig. 8 Simulated structure (red) of TcAChE in bulk water (A) and TcAChE adsorbed on the 7% dissociated NH_2-SAM (B); on the 7% dissociated COOH-SAM (C); on the 25% dissociated NH_2-SAM (D); and on the 25% dissociated COOH-SAM (E) superimposed on its crystal structure (green).

studies.[45,60] Meanwhile, it is obvious that the total interaction energies are stronger on positively charged surfaces (NH_2-SAM) compared with those on negatively charged surfaces (COOH-SAM), which is mainly caused by the net negative charge of TcAChE, $-7e$. On a negatively charged SAM surface, due to the electrostatic repulsion, the electrostatic interaction energy decreases with the increase of the SCD; however, it rises up obviously on positively charged SAMs. The vdW interaction energy changes slightly on the oppositely charged surfaces. This further demonstrates that the adsorption behaviour of TcAChE on charged surfaces is dominated by the electrostatic interactions between TcAChE and charged SAMs.

Active-site gorge

The substrate transport pathway (*i.e.*, the active-site gorge, also called a substrate tunnel), plays an essential role in protein functioning, including mediating the transport of ions or molecules across biological membranes[75] and facilitating the exchange of the substrate (*i.e.*, small molecules and ions) between the buried active site in enzymes and the bulk solvent.[76,77] The understanding of the structure–function relationships of these proteins was helpful for the design of new inhibitors and construction of improved biocatalysts or biosensors. For TcAChE, the substrate tunnel (as shown in Fig. 1A) was important for the enzyme catalytic activity. The final active-site gorge configurations of TcAChE on both charged SAMs (*i.e.*, NH_2-SAM and COOH-SAM) are displayed in Fig. 4.

It can be seen from Fig. 4A and C that TcAChE could be adsorbed on NH_2-SAM surfaces with its active-site gorge near the surface; however, on COOH-SAM surfaces, the active-site gorges of TcAChE were far away from the electrode surfaces (as shown in Fig. 4B and D). For both charged surfaces, the orientations of the active-site gorge show no obvious change with the increase of the SCD, indicating that TcAChE could orderly adsorb on charged surfaces, regardless of the SCD of electrode surfaces. It can also be found that the positively charged surface could reduce the distance among the catalytically active site, substrate tunnel of TcAChE and electrode surface. In a previous experimental study,[28] it has been reported that a positively charged surface (CNT-NH_2) showed higher affinity to an enzyme substrate (acetylthiocholine chloride), which indicates that the enzyme substrate needs to be transferred to the active-site from the electrode surface by the active-site gorge. So, the orientation with the active-site gorge towards the electrode surface is favourable for the transportation of enzyme substrates. Furthermore, the substrate tunnel of TcAChE is long and narrow when TcAChE is adsorbed on COOH-SAM surfaces. In contrast, a shorter and wider substrate tunnel is presented on NH_2-SAM surfaces, which is helpful for the substrate (acetylcholine) to reach the active-site and to induce faster electron transfer and more efficient reaction.

To further reveal the influence of charged surfaces on the substrate tunnel of TcAChE, several significant characteristic parameters for the substrate tunnels, including the tunnel length, radius of the tunnel bottleneck (indicates the maximum radius of the narrowest region of the tunnel), tunnel curvature and tunnel cost, were calculated and are shown in Table 2. The result of TcAChE in bulk solution was chosen as the reference system. Usually, the tunnel cost which is defined as $c(r,L) = \frac{L}{r^2}$, where L and r are the length and constant radius of a tunnel,[49] depends on the other three parameters, that is, the tunnel cost increases with the increase of the tunnel length, or the decrease of the radius of the tunnel bottleneck and tunnel curvature, and a lower value is favourable for the transportation of enzyme substrates.

It can be seen from Table 2 that in the bulk solution, the tunnel length, radius of the tunnel bottleneck, tunnel curvature and tunnel cost are 1.211 nm, 0.191 nm, 1.167 and 0.300, respectively. For the 7% dissociated NH_2-SAM surface, the tunnel length of TcAChE increases slightly; however, the radius of the tunnel bottleneck also increases and the tunnel curvature decreases compared with those in the bulk, which leads to the tunnel cost reducing to 0.202, and it is 33.7% smaller than that of TcAChE in the bulk. This situation can also be found on the 25% dissociated NH_2-SAM surface. For 7% and 25% dissociated COOH-SAM surfaces, the tunnel lengths of TcAChE increase to 2.197 nm and 1.703 nm, respectively. They are 81.4% and 40.6% larger than that in the bulk (1.211 nm). The tunnel curvatures of the enzyme also increase obviously (1.761 and 1.640), and are 50.9% and 40.5%

larger than that of TcAChE in the bulk (1.167). Furthermore, the radius of the tunnel bottleneck within TcAChE decreases to 0.114 nm and 0.155 nm, respectively. They are 40.3% and 18.8% smaller than that in the bulk (0.191 nm). As a result, the tunnel cost shows a sharp increase, reaching up to 0.691 and 0.511. They are 130.3% and 70.3% larger than that of TcAChE in the bulk (0.300). These results indicate that the positively charged surfaces (NH_2-SAM) can accelerate the substrate transfer with a low tunnel cost, which leads to more efficient biological catalysis. However, it is unfavourable for the substrate transfer and bio-catalysis when TcAChE is adsorbed on the negatively charged surfaces (COOH-SAM) with a high tunnel cost. It can be concluded that positively charged surfaces are more suitable for the immobilization of TcAChE, which also agrees with the previous experimental results[28,34,35] and is also consistent with the protein–surface interaction energies (as shown in Table 1), revealing that TcAChE has a stronger interaction with the positively charged surface.

The key binding sites

To better reveal the key adsorption residues of TcAChE adsorbed on both charged SAM (*i.e.*, NH_2-SAM and COOH-SAM) surfaces with different SCDs, residues of TcAChE in contact with the surface are analysed after the simulations reach equilibrium. When the distance between the surface and any residue atom is within 0.35 nm, these residues containing the contacting atoms are considered as contacting residues. All contacting residues are listed in Table S1.† In order to investigate the adsorption stability of TcAChE on charged surfaces, the corresponding contact maps of residues are also plotted in Fig. S1.† The key binding sites or residues, which have relatively strong interactions with the charged surfaces, are labelled in Fig. 5. Moreover, the interaction energies (*i.e.*, electrostatic and vdW interaction energies) between the key binding residues of TcAChE and both SAM surfaces are computed in detail; the results are presented in Fig. 6.

As illustrated in Fig. 5, for the 7% dissociated NH_2-SAM surface, the key binding sites consist of Asp72, Gly77, Glu82, Glu89, Glu273, Asp276, Asp342 and Ser343. They are almost negatively charged residues except Gly77 and Ser343, and these residues come in contact with the NH_2-SAM surface in less than 30 ns and then stay on the surface till the end of AAMD simulations (as shown in Fig. S1A†). Additionally, all contact residues are located in the main negative potential region (as shown in Fig. 1B), which indicates that the major negatively charged patch of TcAChE is close to the NH_2-SAM surface. To further investigate the individual residue contribution to adsorption, the interaction energies (*i.e.*, electrostatic and vdW interaction energies) between key binding residues of TcAChE and SAMs were calculated, and the results are summarized in Fig. 6. As can be seen from Fig. 6A, the negatively charged residues, including Asp72, Glu82, Glu89, Glu273, and Asp276, strongly interact with the NH_2-SAM surface. The strong interaction energy is majorly contributed by the electrostatic interactions. This shows that the adsorption of TcAChE on the positively charged surface is dominated by electrostatic interactions, which is consistent with the results in the section "Adsorption orientation and interaction energy" (as shown in Table 1). For the TcAChE adsorption on the 25% dissociated NH_2-SAM surface, the strong interaction with the surface is dominated by the negatively charged residues Asp72, Glu73, Glu273, Asp276, Asp342, Glu344, Glu350, and Asp351 (as labelled in Fig. 5C). The number of key residues and protein–surface electrostatic interactions increase with the increase in the SCD as TcAChE has a net charge of $-7e$, and all the key residues are also located within the main negative potential region of TcAChE and adsorbed stably on the surface within 15 ns till the end of simulation (as illustrated in Fig. S1C†). Moreover, as shown in Fig. 2C and E, almost the same "end-on" orientation can be found on 7% and 25% dissociated NH_2-SAM surfaces, and the total number of contact residues is also equal (as presented in Table S1†). This indicates that TcAChE could be immobilized efficiently on both positively charged surfaces.

For the adsorption of TcAChE on 7% dissociated COOH-SAM, the key contact residues are Lys107, Lys192, Arg220, Lys316, Lys413, Asn416, His486, Lys491, and Lys498 (as illustrated in Fig. 5B and 6B). It can also be seen from Fig. S1B† that all these residues maintain their adsorption state after 20 ns. It is noteworthy to point out that all key binding sites are almost positively charged residues except Asn416. The strong interaction energies are still electrostatically dominant, which indicates that the adsorption of TcAChE on the negatively charged surface is also controlled by the electrostatic interactions between TcAChE and the surface. It agrees with the conclusion in our previous studies that the driving force inducing protein adsorption on charged surfaces is the electrostatic interaction.[45,60,78] Furthermore, all positively charged key contact residues are located within the main positive potential region (as illustrated in Fig. 1C). This suggests that TcAChE adsorbed on the COOH-SAM with its positively charged patch approaching the negative surface. Therefore, the orientation of TcAChE on the negatively charged surface is controlled by the synergy of the electric dipole[38] and the distribution of charged patches, which is the reason why negatively charged TcAChE could adsorb stably on the negatively charged surface. For the adsorption of TcAChE on the 25% dissociated COOH-SAM, the key binding sites are almost the same except Arg221 and Phe414 (as depicted in Fig. 5D). They come in contact with the surface within 10 ns, and then stay there stably (as illustrated in Fig. S1D†). Although the interaction energies between the protein and the surface (as shown in Fig. 6D) increase obviously with the increase of the SCD, the adsorption orientation is not changed ("back-on", as shown in Fig. 2F). In general, under the regulation of the electric dipole and the distribution of charged patches, TcAChE could be immobilized on both charged surfaces with different SCDs.

Protein conformational stability

To quantitatively characterize the structural stability of TcAChE on different charged SAM surfaces, the dipole moment, gyra-

tion radius (R_{gyr}), eccentricity, root-mean-square deviation (RMSD) of the backbone atoms of TcAChE, root-mean-square fluctuation (RMSF) of each residue, and superimposed structures during MD simulations were calculated and analysed in detail. The averaged properties of TcAChE in bulk solution and that adsorbed on the SAM surface are summarized in Table 3 by statistical analysis of the last 60 ns MD simulation trajectories.

RMSD, RMSF and dipole moment

The RMSD value is calculated by comparing the crystal and simulated structures of TcAChE during AAMD simulations, and the back-bone atoms and all atoms of TcAChE were considered at the same time. The back-bone RMSD was used to quantitatively characterize the overall natural structural stability of TcAChE in all AAMD simulations. At the same time, in order to verify that the slight secondary structural change was caused by the side chain and flexible structures (*i.e.*, turns, coils and terminals) rather than the back-bone structure, we further calculated the all-atom RMSD. The results are presented in Table 3. The time evolution of the RMSD during the whole processes of MD simulations is also plotted in Fig. S2.† It can be seen that values of the RMSD remain unchanged since 120 ns, which indicates that all systems have reached the equilibrium state and 200 ns simulation is sufficient. The RMSD value of TcAChE in bulk solution was used as the reference. As depicted in Table 3, the backbone RMSD value is 0.20 nm; however, the value of the RMSD of all-atoms increases to 0.25, which indicates that the slight structural fluctuation of TcAChE in the bulk was mainly caused by the side chains of the protein, and the back-bone structure remains stable. For both charged SAMs, the RMSD values were almost equal to that of TcAChE in the bulk, except the 7% dissociated COOH-SAM surface which shows a lower RMSD value because of the relatively low protein–surface interactions compared with those on positively charged SAM surfaces, which imply that the native conformation of TcAChE is preserved during adsorption.

The residue-based RMSF of the backbone atom was calculated to further investigate the local conformational change of TcAChE, which can be used to specifically identify the regions of a protein that undergoes structural fluctuations during the simulation. As illustrated in Fig. 7, for most residues of TcAChE in the bulk and those adsorbed on SAMs with different SCDs, the values of RMSF are less than 0.2 nm, and only some residues that are located within the relatively flexible secondary structure (*i.e.*, N-terminal and C-terminal, coil, loop and turn structures) of TcAChE experience larger conformational changes and a similar phenomenon has been found in previous studies.[60,78] In bulk solution, as can be seen from Fig. 7A, the turn residues 73–78, 377–381, and 429–430, coil residues 283–285 and 431–432 and C-terminal of TcAChE show relatively larger RMSF values. When adsorbed on the 7% dissociated NH_2-SAM surface, the coil residues 283–284, 413–416, and 488–489, turn residues 378–380 and 485–487 and C-terminal exhibit larger RMSF fluctuations (Fig. 7B). The coil residues 71–72, 344, and 488–489, turn residues 73–79, 340–343, 377–382, and 486–487 and C-terminal of TcAChE adsorbed on the 7% dissociated COOH-SAM display larger RMSF values (as shown in Fig. 7C). Similarly, for TcAChE adsorption on the 25% dissociated NH_2-SAM, coil residues 71–72, 85–89, 414–416, and 489–491, turn residues 73–78 and 377–383 and C-terminal present higher values of RMSF (as illustrated in Fig. 7D). For the 25% dissociated COOH-SAM surface, larger RMSF values of TcAChE are found on the coil residues 84–89 and 431–434, turn residues 378–383 and 427–430 and C-terminal (show in Fig. 7E). The results indicate that slight structural changes of TcAChE mainly occur on the relatively flexible turns, coils and terminal structure, and the back-bone secondary structures were quite stable in all simulation processes.

The dipole moment is usually used to represent the distribution of protein charges and characterize the conformational changes of the protein. As shown in Table 3, the dipole moment of TcAChE in the bulk has a large value of 1976 D, which is caused by the asymmetrical distribution of charged residues (as shown in Fig. 1B and C). When adsorbed on 7% and 25% dissociated NH_2-SAMs, the values of dipole moments increase to 2130 D and 2279 D, respectively. They are 7.8% and 15.3% larger than that of TcAChE in the bulk. Meanwhile, the dipole moment of TcAChE on 7% and 25% dissociated COOH-SAMs also increase to 2051 D and 2113 D, respectively, and they are 3.8% and 6.9% larger than that in bulk solution. These results indicate that the dipole moment of TcAChE adsorbed on both charged surfaces increases with the increase of the SCD. In other words, TcAChE experiences slight structural changes when immobilized on charged SAMs, and these changes mainly occur on the flexible turn and coil structures of the protein, which also indicates that the backbone secondary structure of TcAChE is not significantly affected by the charged surface during simulations.

Gyration radius, eccentricity, and superimposed structures

The eccentricity and R_{gyr} were also calculated to monitor the overall shape of TcAChE during AAMD simulations. The results are shown in Table 3. The R_{gyr} of a protein refers to the mass weighted root-mean-square average distance of all atoms in a protein from its centre of mass. As depicted in Table 3, the calculated average R_{gyr} values are 2.35 nm, 2.33 nm, 2.32 nm, and 2.33 nm for TcAChE adsorbed on 7% and 25% dissociated NH_2-SAMs and 7% and 25% dissociated COOH-SAMs, respectively. They are very close to that of TcAChE in bulk solution (2.33 nm). The results demonstrate that the overall size of TcAChE does not substantially expand or shrink after immobilization in all cases. Furthermore, eccentricity, which is defined as $1 - I_{ave}/I_{max}$, where I_{ave} represents the average of three principal moments of inertia and I_{max} is the maximal principal moment of inertia, was also calculated to characterize the structural change of the protein during AAMD simulations, as shown in Table 3. The eccentricity value of TcAChE in bulk solution is 0.18, close to zero. It suggests that TcAChE is a sphere-like protein.[44,60] When

TcAChE adsorbed on both charged surfaces, the eccentricity values hardly changed. This indicates that the charged surface at different SCDs does not affect the overall shape of TcAChE during the immobilization process. Finally, in order to clearly and visually observe the overall secondary structural changes of TcAChE in the bulk and that adsorbed on different charged surfaces, the final simulated structures are superimposed onto its crystal structure (the structure before simulation that is adopted from the Protein Data Bank, http://www.rcsb.org/) and the results are shown in Fig. 8. It can be seen that the slight secondary structural change can be found in the flexible structures (*i.e.*, turns, coils and terminals) of TcAChE. Nevertheless, the basic backbone structure of TcAChE is well preserved in all cases, and this kind of change does not affect obviously the catalytic activity of TcAChE, which is consistent with the aforementioned data analyses of RMSD, RMSF, R_{gyr} and eccentricity.

Conclusions

In this work, multiscale simulations, including Parallel Tempering Monte Carlo and all-atom molecular dynamics, have been performed to investigate the molecular adsorption mechanism (*i.e.*, adsorption orientation, conformation and effective direct electron transfer) of TcAChE on charged surfaces (NH_2-SAM and COOH-SAM). The effect of the surface charge density on the adsorption was also studied. The simulation results indicate that the immobilization of TcAChE on a positively charged surface is favourable for maintaining the bioactivity of the enzyme and accelerating the direct electron transfer between TcAChE and surfaces, which agrees well with previous experimental results.

The main driving forces of TcAChE adsorbed on both charged SAM surfaces are the synergy of electrostatic and vdW interactions and the electrostatic interactions play the dominant role. For the adsorption of TcAChE on a positively charged surface, the active-site gorge orients toward the surface with the "end-on" orientation, the main negative potential patch adsorbs directly on the surface, and the active centre is close to the surface, which makes the path of the electron and enzyme substrate transfer shorter, and further induces a faster DET and more efficient reaction. In contrast, TcAChE adsorbed on a negatively charged surface with the "back-on" orientation. The main positive potential patch serves as the landing point of adsorption; the active-site gorge orients toward the solution. Active residues are far away from the electrode surface, and it is not good for the DET between the enzyme and surface. Furthermore, the tunnel cost for the substrate is higher than that of TcAChE on the positively charged surface. The results indicate that the immobilization of TcAChE on the positively charged surface is better for TcAChE-based biofuel cells and amperometric biosensors.

Moreover, the conformational changes of TcAChE in bulk solution and on both charged surfaces are also evaluated. The RMSD, RMSF, dipole moment, gyration radius, eccentricity and superimposed structures are analyzed in detail. The results indicate that no significant variation is observed, except the slight secondary structural fluctuation on the relatively flexible portions (*i.e.*, turns, coils and terminals) of the protein for all systems. The overall native back-bone structure of TcAChE is well maintained after adsorption. This work helps understand the adsorption mechanism of TcAChE on charged surfaces at the molecular level and also provides some new insights into the design and development of rapid, reliable TcAChE-based bio-electrodes and organophosphorus pesticide biosensors.

Conflicts of interest

The authors declare no competing financial interest.

Acknowledgements

Support from the National Natural Science Foundation of China (No. 21776093, 21376089 and 21706197), the National Key Basic Research Program of China (No. 2013CB733500) and Guangdong Science Foundation (No. 2014A030312007) is gratefully acknowledged. An allocation time from the SCUTGrid at the South China University of Technology is gratefully acknowledged.

References

1 H. Dvir, I. Silman, M. Harel, T. L. Rosenberry and J. L. Sussman, *Chem.-Biol. Interact.*, 2010, **187**, 10–22.
2 H. Dvir, H. L. Jiang, D. M. Wong, M. Harel, M. Chetrit, X. C. He, G. Y. Jin, G. L. Yu, X. C. Tang, I. Silman, D. L. Bai and J. L. Sussman, *Biochemistry*, 2002, **41**, 10810–10818.
3 B. E. Mileson, J. E. Chambers, W. L. Chen, W. Dettbarn, M. Ehrich, A. T. Eldefrawi, D. W. Gaylor, K. Hamernik, E. Hodgson, A. G. Karczmar, S. Padilla, C. N. Pope, R. J. Richardson, D. R. Saunders, L. P. Sheets, L. G. Sultatos and K. B. Wallace, *Toxicol. Sci.*, 1998, **41**, 8–20.
4 M. Stoytcheva, V. Gochev and Z. Velkova, *Curr. Anal. Chem.*, 2016, **12**, 37–42.
5 P. Kumar, K.-H. Kim and A. Deep, *Biosens. Bioelectron.*, 2015, **70**, 469–481.
6 C. S. Pundir and N. Chauhan, *Anal. Biochem.*, 2012, **429**, 19–31.
7 M. Stoytcheva, *Intell. Biosens.*, 2010, 217–230.
8 D. Harshit, K. Charmy and P. Nrupesh, *Food Chem.*, 2017, **230**, 448–453.
9 J. Xie, T. Liu, G. Song, Y. Hu and C. Deng, *Chromatographia*, 2013, **76**, 535–540.
10 M. J. Tan, Z.-Y. Hong, M.-H. Chang, C.-C. Liu, H.-F. Cheng, X. J. Loh, C.-H. Chen, C.-D. Liao and K. V. Kong, *Biosens. Bioelectron.*, 2017, **96**, 167–172.
11 Y. Z. Piao, Y. J. Kim, Y. A. Kim, H.-S. Lee, B. D. Hammock and Y. T. Lee, *J. Agric. Food Chem.*, 2009, **57**, 10004–10013.

12 R. Bala, R. K. Sharma and N. Wangoo, *Anal. Bioanal. Chem.*, 2016, **408**, 333–338.
13 P. Raghu, T. Madhusudana Reddy, K. Reddaiah, B. E. Kumara Swamy and M. Sreedhar, *Food Chem.*, 2014, **142**, 188–196.
14 E. A. Songa and J. O. Okonkwo, *Talanta*, 2016, **155**, 289–304.
15 M. Stoytcheva, R. Zlatev, Z. Velkova and B. Valdez, *Pesticides-Strategies for Pesticides Analysis*, 2011, pp. 359–372.
16 C. Gutiérrez-Sánchez, M. Pita, C. Vaz-Domínguez, S. Shleev and A. L. De Lacey, *J. Am. Chem. Soc.*, 2012, **134**, 17212–17220.
17 A. Sassolas, L. J. Blum and B. D. Leca-Bouvier, *Biotechnol. Adv.*, 2012, **30**, 489–511.
18 M. Kesik, F. Ekiz Kanik, J. Turan, M. Kolb, S. Timur, M. Bahadir and L. Toppare, *Sens. Actuators, B*, 2014, **205**, 39–49.
19 H. Patel, D. Rawtani and Y. K. Agrawal, *Trends Food Sci. Technol.*, 2019, **85**, 78–91.
20 D. Du, S. Chen, J. Cai and A. Zhang, *Biosens. Bioelectron.*, 2007, **23**, 130–134.
21 K. Khaldi, S. Sam, A. C. Gouget-Laemmel, C. Henry de Villeneuve, A. Moraillon, F. Ozanam, J. Yang, A. Kermad, N. Ghellai and N. Gabouze, *Langmuir*, 2015, **31**, 8421–8428.
22 S. Sotiropoulou, D. Fournier and N. A. Chaniotakis, *Biosens. Bioelectron.*, 2005, **20**, 2347–2352.
23 R. R. Dutta and P. Puzari, *Biosens. Bioelectron.*, 2014, **52**, 166–172.
24 J. S. Van Dyk and B. Pletschke, *Chemosphere*, 2011, **82**, 291–307.
25 J. Diao, X. Yu, L. Ma, Y. Li and Y. Sun, *Bioconjugate Chem.*, 2018, **29**, 1703–1713.
26 F. Meder, H. Hintz, Y. Koehler, M. M. Schmidt, L. Treccani, R. Dringen and K. Rezwan, *J. Am. Chem. Soc.*, 2013, **135**, 6307–6316.
27 M. Xiao, S. Wei, J. Chen, J. Tian, C. L. Brooks Iii, E. N. G. Marsh and Z. Chen, *J. Am. Chem. Soc.*, 2019, **141**, 9980–9988.
28 G. Yu, W. Wu, Q. Zhao, X. Wei and Q. Lu, *Biosens. Bioelectron.*, 2015, **68**, 288–294.
29 C. Gutierrez-Sanchez, A. Ciaccafava, P. Y. Blanchard, K. Monsalve, M. T. Giudici-Orticoni, S. Lecomte and E. Lojou, *ACS Catal.*, 2016, **6**, 5482–5492.
30 B. Ding, J. Jasensky, Y. Li and Z. Chen, *Acc. Chem. Res.*, 2016, **49**, 1149–1157.
31 K. Srinivasan, S. Banerjee, S. Parimal, L. Sejergaard, R. Berkovich, B. Barquera, S. Garde and S. M. Cramer, *Langmuir*, 2017, **33**, 10851–10860.
32 P. Olejnik, B. Palys, A. Kowalczyk and A. M. Nowicka, *J. Phys. Chem. C*, 2012, **116**, 25911–25918.
33 F. Meder, T. Daberkow, L. Treccani, M. Wilhelm, M. Schowalter, A. Rosenauer, L. Mädler and K. Rezwan, *Acta Biomater.*, 2012, **8**, 1221–1229.
34 G. Liu and Y. Lin, *Anal. Chem.*, 2006, **78**, 835–843.
35 P. Zhang, T. Sun, S. Rong, D. Zeng, H. Yu, Z. Zhang, D. Chang and H. Pan, *Bioelectrochemistry*, 2019, **127**, 163–170.
36 M. Guler, V. Turkoglu and Z. Basi, *Electrochim. Acta*, 2017, **240**, 129–135.
37 F. E. Kanik, M. Kolb, S. Timur, M. Bahadir and L. Toppare, *Int. J. Biol. Macromol.*, 2013, **59**, 111–118.
38 J. Zhou, J. Zheng and S. Jiang, *J. Phys. Chem. B*, 2004, **108**, 17418–17424.
39 T. Wei, M. A. Carignano and I. Szleifer, *J. Phys. Chem. B*, 2012, **116**, 10189–10194.
40 Q. Wang, C. Zhao, J. Zhao, J. Wang, J.-C. Yang, X. Yu and J. Zheng, *Langmuir*, 2010, **26**, 3308–3316.
41 X. Quan, J. Liu and J. Zhou, *Curr. Opin. Colloid Interface Sci.*, 2019, **41**, 74–85.
42 B. Li, D. R. Bell, Z. Gu, W. Li and R. Zhou, *Carbon*, 2019, **146**, 257–264.
43 C. Peng, J. Liu and J. Zhou, *J. Phys. Chem. C*, 2015, **119**, 20773–20781.
44 D. Zhao, C. Peng and J. Zhou, *Phys. Chem. Chem. Phys.*, 2015, **17**, 840–850.
45 J. Liu, Y. Xie, C. Peng, G. Yu and J. Zhou, *J. Phys. Chem. B*, 2017, **121**, 10610–10617.
46 Y. Xie, J. Zhou and S. Jiang, *J. Chem. Phys.*, 2010, **132**, 065101.
47 J. L. Sussman, M. Harel, F. Frolow, C. Oefner, A. Goldman, L. Toker and I. Silman, *Science*, 1991, **253**, 872.
48 W. L. DeLano, *CCP4 Newsletter On Protein Crystallography*, 2002, vol. 40, pp. 82–92.
49 E. Chovancova, A. Pavelka, P. Benes, O. Strnad, J. Brezovsky, B. Kozlikova, A. Gora, V. Sustr, M. Klvana, P. Medek, L. Biedermannova, J. Sochor and J. Damborsky, *PLoS Comput. Biol.*, 2012, **8**, e1002708.
50 A. Pavelka, E. Sebestova, B. Kozlikova, J. Brezovsky, J. Sochor and J. Damborsky, *IEEE/ACM Trans. Comput. Biol. Bioinf.*, 2016, **13**, 505–517.
51 E. F. Pettersen, T. D. Goddard, C. C. Huang, G. S. Couch, D. M. Greenblatt, E. C. Meng and T. E. Ferrin, *J. Comput. Chem.*, 2004, **25**, 1605–1612.
52 Y. Levy and J. N. Onuchic, *Annu. Rev. Biophys. Biomol. Struct.*, 2006, **35**, 389–415.
53 B. Hess, C. Kutzner, D. van der Spoel and E. Lindahl, *J. Chem. Theory Comput.*, 2008, **4**, 435–447.
54 A. D. MacKerell, D. Bashford, M. Bellott, R. L. Dunbrack, J. D. Evanseck, M. J. Field, S. Fischer, J. Gao, H. Guo, S. Ha, D. Joseph-McCarthy, L. Kuchnir, K. Kuczera, F. T. K. Lau, C. Mattos, S. Michnick, T. Ngo, D. T. Nguyen, B. Prodhom, W. E. Reiher, B. Roux, M. Schlenkrich, J. C. Smith, R. Stote, J. Straub, M. Watanabe, J. Wiórkiewicz-Kuczera, D. Yin and M. Karplus, *J. Phys. Chem. B*, 1998, **102**, 3586–3616.
55 Q. Wang, J. Zhao, X. Yu, C. Zhao, L. Li and J. Zheng, *Langmuir*, 2010, **26**, 12722–12732.
56 S. E. Feller and A. D. MacKerell, *J. Phys. Chem. B*, 2000, **104**, 7510–7515.
57 J. J. Gray, *Curr. Opin. Struct. Biol.*, 2004, **14**, 110–115.

58 M. Agashe, V. Raut, S. J. Stuart and R. A. Latour, *Langmuir*, 2005, **21**, 1103–1117.
59 J. Zhou, S. Chen and S. Jiang, *Langmuir*, 2003, **19**, 3472–3478.
60 S. Yang, J. Liu, X. Quan and J. Zhou, *Langmuir*, 2018, **34**, 9818–9828.
61 S. Patel and C. L. Brooks Iii, *J. Comput. Chem.*, 2004, **25**, 1–16.
62 W. L. Jorgensen, J. Chandrasekhar, J. D. Madura, R. W. Impey and M. L. Klein, *J. Chem. Phys.*, 1983, **79**, 926–935.
63 W. Hoover, *Canonical Dynamics: Equilibrium Phase-Space Distributions*, 1985.
64 I.-C. Yeh and M. L. Berkowitz, *J. Chem. Phys.*, 1999, **111**, 3155–3162.
65 B. Hess, *J. Comput. Chem.*, 1997, **18**, 1463–1472.
66 W. Humphrey, A. Dalke and K. Schulten, *J. Mol. Graphics*, 1996, **14**, 33–38.
67 C. Léger and P. Bertrand, *Chem. Rev.*, 2008, **108**, 2379–2438.
68 A. L. Ghindilis, P. Atanasov and E. Wilkins, *Electroanalysis*, 1997, **9**, 661–674.
69 F. M. Boubeta, G. Soler-Illia and M. Tagliazucchi, *Langmuir*, 2018, **34**, 15727–15738.
70 J. Liu, C. Peng, G. Yu and J. Zhou, *Langmuir*, 2015, **31**, 10751–10763.
71 C. Peng, J. Liu, D. Zhao and J. Zhou, *Langmuir*, 2014, **30**, 11401–11411.
72 D. Zhao, L. Li and J. Zhou, *Appl. Surf. Sci.*, 2018, **428**, 825–834.
73 D. Zhao, L. Li, D. He and J. Zhou, *Appl. Surf. Sci.*, 2016, **377**, 324–334.
74 G. Yu, J. Liu and J. Zhou, *J. Phys. Chem. B*, 2014, **118**, 4451–4460.
75 A. Miyazawa, Y. Fujiyoshi and N. Unwin, *Nature*, 2003, **423**, 949–955.
76 B. M. Barney, M. G. Yurth, P. C. Dos Santos, D. R. Dean and L. C. Seefeldt, *J. Biol. Inorg. Chem.*, 2009, **14**, 1015–1022.
77 S. M. Marques, L. Daniel, T. Buryska, Z. Prokop, J. Brezovsky and J. Damborsky, *Med. Res. Rev.*, 2017, **37**, 1095–1139.
78 J. Liu, G. Yu and J. Zhou, *Chem. Eng. Sci.*, 2015, **121**, 331–339.